

The Rad51/RadA N-Terminal Domain Activates Nucleoprotein Filament ATPase Activity

Vitold E. Galkin,¹ Yan Wu,² Xiao-Ping Zhang,³
Xinguo Qian,² Yujiong He,² Xiong Yu,¹
Wolf-Dietrich Heyer,³ Yu Luo,²
and Edward H. Egelman^{1,*}

¹Department of Biochemistry and Molecular Genetics
University of Virginia
Box 800733

Charlottesville, Virginia 22908

²Department of Biochemistry
University of Saskatchewan
A3 Health Sciences Building
107 Wiggins Road
Saskatoon, Saskatchewan
Canada S7N 5E5

³Section of Microbiology
Section of Molecular and Cellular Biology
Center for Genetics and Development
University of California, Davis
Davis, California 95616

Summary

Proteins in the RecA/RadA/Rad51 family form helical filaments on DNA that function in homologous recombination. While these proteins all have the same highly conserved ATP binding core, the RadA/Rad51 proteins have an N-terminal domain that shows no homology with the C-terminal domain found in RecA. Both the Rad51 N-terminal and RecA C-terminal domains have been shown to bind DNA, but no role for these domains has been established. We show that RadA filaments can be trapped in either an inactive or active conformation with respect to the ATPase and that activation involves a large rotation of the subunit aided by the N-terminal domain. The G103E mutation within the yeast Rad51 N-terminal domain inactivates the filament by failing to make proper contacts between the N-terminal domain and the core. These results show that the N-terminal domains play a regulatory role in filament activation and highlight the modular architecture of the recombination proteins.

Introduction

The *recA* gene was identified in *E. coli* more than 40 years ago (Clark and Margulies, 1965) and has served as a model system for understanding homologous genetic recombination. RecA is involved in recombination, DNA repair, activation of the SOS response (Courcelle et al., 2001), cleavage of phage repressors, and mutagenic translesion synthesis (Schlacher et al., 2005), among other activities. A great deal has been learned about how RecA functions from in vitro DNA strand-exchange reactions, where this protein can catalyze the transfer of a DNA strand between two homologous molecules (Kowalczykowski and Eggleston, 1994). The active form

of RecA in this reaction is a helical filament formed on DNA. Interest in bacterial RecA was enhanced by the discovery that eukaryotic cells encode a homologous protein, Rad51 (Shinohara et al., 1992; Aboussekhra et al., 1992), that forms similar helical nucleoprotein filaments on DNA as those formed by RecA (Ogawa et al., 1993). A second eukaryotic RecA-like protein, the meiosis-specific Dmc1, also forms such nucleoprotein filaments (Sehorn et al., 2004). With the discovery that archaea encode a RadA protein (Sandler et al., 1996) and that RadA-DNA filaments are also similar to RecA-, Rad51-, and Dmc1-DNA filaments (Yang et al., 2001), it is apparent that all of the major kingdoms of life encode a recombination system that is based upon a similar filamentous architecture.

A detailed mechanistic picture of how RecA-like filaments function in recombination and other reactions is still lacking despite much effort invested in this area. The first crystal structure of RecA (Story et al., 1992) provided a high-resolution picture of a RecA filament, but in the absence of DNA. This crystal structure is now understood to be a compressed, inactive state (VanLoock et al., 2003). More recent crystal structures of archaeal RadA (Wu et al., 2004) and yeast Rad51 (Conway et al., 2004) show an extended conformation. Crystal structures of RecA (Story et al., 1992; King and Bell, 2004a, 2004b; Rajan and Bell, 2004; Datta et al., 2000, 2003a, 2003b), RadA (Shin et al., 2003; Wu et al., 2004), Rad51 (Conway et al., 2004), and Dmc1 (Kinebuchi et al., 2004) have all revealed a nucleotide binding core that is highly conserved among different proteins from different species. In fact, this same nucleotide binding core was also seen in the F1-ATPase, and the rms deviation for the superposition of 120 C- α residues within this core between bacterial RecA and the bovine F1-ATPase is less than 2 Å (Abrahams et al., 1994). Despite the high degree of structural conservation of the cores, the modular architecture of the RecA protein (and filament) is different from that of RadA, Rad51, and Dmc1. RecA has a C-terminal domain that has no homology, either at the level of sequence or structure, with the conserved N-terminal domains contained within RadA, Rad51, and Dmc1. Nevertheless, there are a number of parallels between these two different domains. Both have been shown to bind DNA (Aihara et al., 1997, 1999). Approximately 25 C-terminal residues in RecA have not been seen in crystal structures, presumably due to disorder, while approximately 15 N-terminal residues in human Rad51 (Aihara et al., 1999) and 79 residues in a unique yeast Rad51 N-terminal extension (Conway et al., 2004) have been suggested to be disordered. Crystal structures and electron microscopy have shown that the relation between both the RadA/Rad51/Dmc1 N-terminal domain, on the one hand, and the RecA C-terminal domain, on the other, and the relatively invariant nucleotide binding core can be quite variable (Rajan and Bell, 2004; Shin et al., 2003; Yang et al., 2001; VanLoock et al., 2003; Kinebuchi et al., 2004).

We have used archaeal RadA and yeast Rad51 to look at structure/function relations involving the N-terminal domain. We have done this by creating a RadA protein

*Correspondence: egelman@virginia.edu

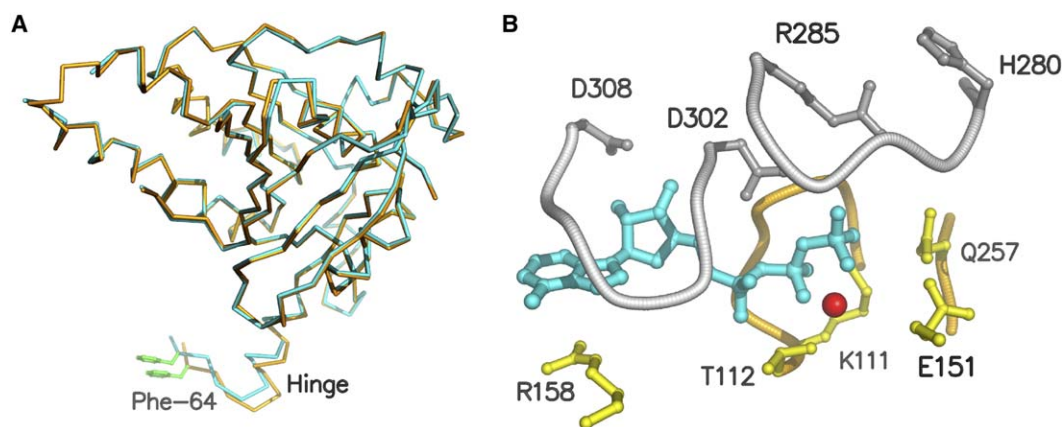


Figure 1. Crystal Structure of the RadA- Δ 62 Fragment

(A) The RadA- Δ 62 conformation (cyan) is essentially identical to the structure of the corresponding core in the full-length protein (gold), except for the polymerization motif around Phe-64 and a short helical hinge.

(B) The ATPase site of the RadA- Δ 62 filament resembles that of the previously determined full-length RadA structure. The AMP-PNP (in cyan) is found between two adjacent protomers. The yellow protomer contributes the triphosphate-wrapping P loop, base-stacking Arg-158, and the catalytic Glu-151 and Gln-257. The gray protomer contacts the ATP analog through the ATP cap (residues Asp-302 to Asp-308) and the C-terminal elbow of the L2 region (residues His-280 to Arg-285). The magnesium ion is shown in red.

missing 62 N-terminal residues (RadA- Δ 62), examining the structure of this protein by X-ray crystallography and electron microscopy, and relating this to the biochemical activity of the fragment. We have also used electron microscopy to examine the structure of nucleoprotein filaments formed by the yeast Rad51-G103E mutant protein. Residue 103 is in the N-terminal domain of yeast Rad51 (which corresponds to the highly conserved G23 in MvRadA), and a previous study showed that the G103E mutant inactivated the protein with respect to both ATPase and DNA strand exchange activity (Zhang et al., 2005). The studies of both RadA- Δ 62 and RAD51-G103E lead to a common conclusion: the N-terminal domain in these proteins plays a crucial role in coordinating the ATPase activity of the catalytic core, which involves rotations of the core within the filaments.

Results

Crystal Structure of RadA- Δ 62

The RadA fragment lacking the N-terminal domain, RadA- Δ 62, crystallized in the P6₁ space group, forming a filament in the crystal with six subunits per turn of a 91 Å pitch right-handed helix. This helical crystallographic arrangement is similar to that seen for the full-length protein, except that the helical pitch of the full-length protein was \sim 107 Å (Wu et al., 2004). The RadA- Δ 62 structure superimposed quite well on the corresponding core of the full-length RadA protein (Figure 1A), except for a shift by several Angstroms in the polymerization motif (Pellegriani et al., 2002) containing Phe64 and the adjacent hinge region. This shift reflects the change in helical pitch between the two structures and shows that deformation of this hinge region is involved in the variable pitch observed for all RecA/RadA/Rad51 filaments.

The ATP binding pocket is formed by the interface between two protomers in the filament, as previously shown for the full-length RadA (Wu et al., 2004) and yeast Rad51 (Conway et al., 2004). A nonhydrolyzable

AMP-PNP molecule can be seen bound within this pocket (Figure 1B). The structure thus shows that a helical filament of RadA can be formed, at least in a crystal that properly binds ATP, even in the absence of the N-terminal domain.

In Vitro Activities of RadA- Δ 62

An in vitro assay revealed that RadA- Δ 62 had a DNA-activated ATPase activity that was very similar to that of the full-length protein (Figures 2A and 2B). Since ATPase activity within RecA-like proteins requires filament formation, a mechanistic consequence of the ATP binding and hydrolysis site being located between two subunits in the active form of the helix (Figure 1B), this provides a *prima facie* suggestion that RadA- Δ 62 must be forming filaments on DNA. This has been confirmed by electron microscopy (see below). In contrast to the ATPase activity that is very similar to the full-length protein, RadA- Δ 62 did not exhibit any DNA strand-exchange activity (Figure 2C). This suggests that the N-terminal domain is required for strand exchange but not for filament formation.

Structure of RadA- Δ 62 Filaments

Electron microscopy confirms that the RadA- Δ 62 protein forms filaments on DNA in the presence of ATP (Figure 3C). In the absence of either DNA or ATP, such filaments are not observed (Table 1). While helical striations can be seen in the extended filaments (with a pitch of \sim 100 Å) formed by the full-length protein in the presence of ADP-AIF (Figure 3A) or the more compressed filaments (with a pitch of \sim 70 Å) formed by the full-length protein in the presence of AMP-PNP (Figure 3B), most of the RadA- Δ 62 filaments appear rather featureless (Figure 3C). In a crystal, in the absence of DNA, the full-length protein forms a rather extended filament (107 Å pitch) with AMP-PNP that is in an active conformation (Wu et al., 2004), while the filaments observed by EM of the full-length protein on DNA in the presence of AMP-PNP are much more compressed.

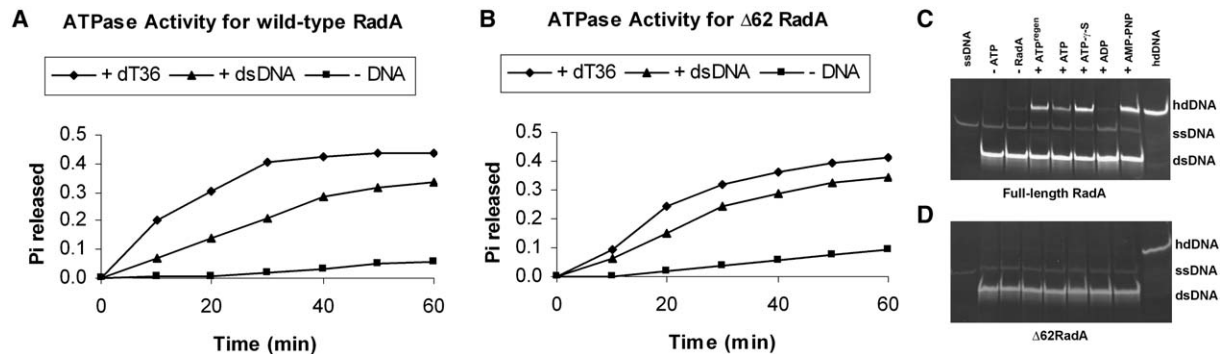


Figure 2. ATPase and DNA Strand Exchange Activities

(A) ATPase activity of full-length MvRadA.
 (B) ATPase activity of RadA-Δ62. There were no significant differences between the two proteins' DNA-dependent ATPase activities.
 (C) The DNA strand-exchange reaction leads to the accumulation of a heteroduplex band (hdDNA) on the ethidium bromide-stained gel. The full-length RadA is active in the presence of all tested nucleoside triphosphates.
 (D) The truncated RadA-Δ62 is inactive.

The iterative helical real space reconstruction (IHRSR) method (Egelman, 2000) was used to analyze both the RadA-Δ62 filaments and the control filaments formed by the full-length protein. Image analysis revealed a helical periodicity of ~50 Å for the relatively featureless RadA-Δ62 filaments. However, this periodicity was determined to arise from a two-start helix having a pitch of ~100 Å and not the one-start helix that is dominant in all other RecA-like filaments. Three-dimensional reconstructions can be compared for the RadA-Δ62 two-start filaments (Figure 4D), the one-start helix formed by the full-length protein in the presence of ADP-AIF with a pitch of 99 Å (Figure 4B), or in the presence of AMP-PNP with a pitch of 71 Å (Figure 4C) and a low-resolution rendering of the crystal structure (Wu et al., 2004) of the full-length protein in the presence of AMP-PNP with a helical pitch of ~107 Å (Figure 4A). In both the full-length protein filaments (Figures 4B and 4C), there is less density seen for the N-terminal domain than in the crystal filament. This can be explained by partial disorder of this domain since we have previously shown that in some states of a *Sulfolobus solfataricus* RadA filament the N-terminal domain was not seen at all after

averaging and three-dimensional reconstruction due to a more extreme disorder (Yang et al., 2001).

The N-terminal domain in the extended state (Figure 4B) appears to be shifted with respect to the position of this domain in the compressed filament (Figure 4C). This N-terminal domain also makes contacts with the ATP binding core of an adjacent subunit in the extended state (red arrow, Figure 4B), but such contacts are lacking in the compressed state (Figure 4C). Fitting the crystal structure of the subunit into both reconstructions yields a simple conclusion: there is a rotation of the subunit by ~30° between these two states (Figure 4E). This is similar to the rotation that has previously been described between the crystal structure of a compressed RecA filament (Story et al., 1992) and fits of atomic models to EM reconstructions of the extended RecA-DNA filaments (VanLoock et al., 2003).

The two-start RadA-Δ62 filaments have approximately eight subunits per turn on each 100 Å pitch helical strand, with a stagger by half a subunit between the two strands. Thus, the two strands are not related by a 2-fold symmetry. Approximately 40% of the segments analyzed from the two-start filaments were used for this

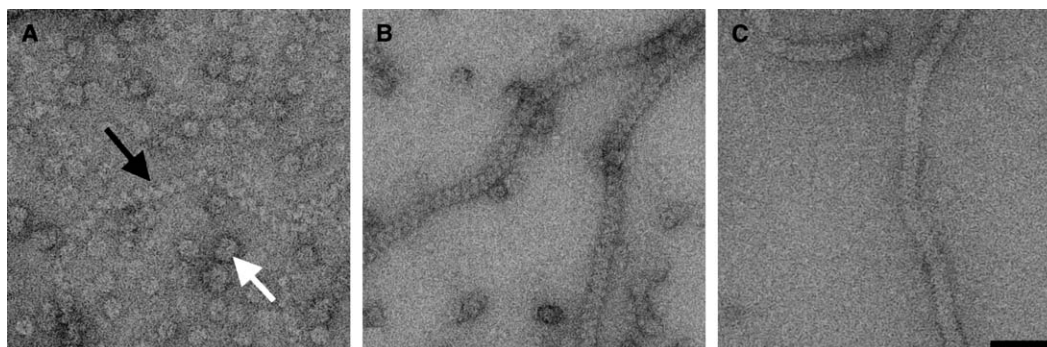


Figure 3. Electron Micrographs of RadA Filaments

Negatively stained RadA filaments formed by the full-length protein (RadA-S2G) (A and B) and filaments formed by the truncated RadA-Δ62 fragment (C). A mixture of filaments (A), black arrow) and rings (A), white arrow) were found in the presence of ADP-AIF, while when AMP-PNP was used, mainly filaments were observed (B). RadA-Δ62-ssDNA filaments complexed with ATP-AIF (C) have no visible modulation of the structure by the deep helical groove, if one compares them with either RadA-S2G-ADP-AIF extended filaments (A) or RadA-AMP-PNP compressed ones (B). These filaments (A) are shown to be two extended filaments that are coiled about each other. The scale bar is 500 Å.

Table 1. Complexes Examined by EM

ATP Cofactor/Complex	AMP-PNP	ATP- γ -S	ATP-AIF	ADP-AIF
yRad51-dsDNA	filaments	filaments	filaments	few filaments
yRad51-G103E-dsDNA	no filaments	no filaments	filaments	few filaments
MvRadA-S2G-dsDNA	filaments	N/A	filaments	filaments
MvRadA Δ 62-dsDNA	filaments	N/A	filaments	filaments
MvRadAS2G-ssDNA	filaments	N/A	few filaments	no filaments
MvRadA Δ 62-ssDNA	filaments	N/A	filaments	filaments

reconstruction. The remaining segments appeared to suffer from disorder, which was consistent with a slippage of one of the strands with respect to the other. In these disordered segments, the relationship between the two strands did not appear to be fixed. Fitting the crystal structure of RadA- Δ 62 into the reconstruction shows that the subunit orientation is more similar to that of the extended state than it is to the compressed one (Figure 4F). The relationship between residues implicated in ATP hydrolysis on two adjacent subunits is shown in Figure 5 for the different conformations observed.

These results show that RadA- Δ 62 can form filaments on DNA, in a novel two-start configuration, that are in an active conformation for hydrolyzing ATP. We first observed these filaments in the presence of dsDNA and wondered whether the two strands might arise from the two strands of DNA. We found that these filaments formed equally well on ssDNA (which were the ones analyzed), so that there is no necessary dependence upon dsDNA being present. The apparent slippage of the two strands with respect to each other provides a mechanism for how subunits might rotate in this

structure during the ATPase cycle. We have also shown, by using the modeling, why the compressed filaments are in an inactive state due to the ATP binding site being rotated out of the pocket between adjacent subunits.

The Yeast Rad51-G103E Mutation

We have used electron microscopy and three-dimensional reconstruction to look at the structural basis for the inactivation of both ATPase and DNA strand-exchange activity by the G103E mutation in yeast Rad51 (Zhang et al., 2005). A striking difference with the wild-type protein is that in the presence of either the slowly hydrolysable ATP analog ATP- γ -S (Figure 6A) or the nonhydrolysable analog AMP-PNP (Figure 6B), the wild-type Rad51 forms filaments on DNA, while the G103E mutation fails to form filaments on either dsDNA or ssDNA with these ATP analogs (Table 1). In the presence of ATP and aluminum fluoride, the G103E mutant readily forms filaments (Figure 6C) that appear very similar to the filaments formed by the wild-type protein under the same conditions (Figure 6D).

Three-dimensional reconstructions of both the wild-type protein filament (Figure 7B) and the G103E mutant

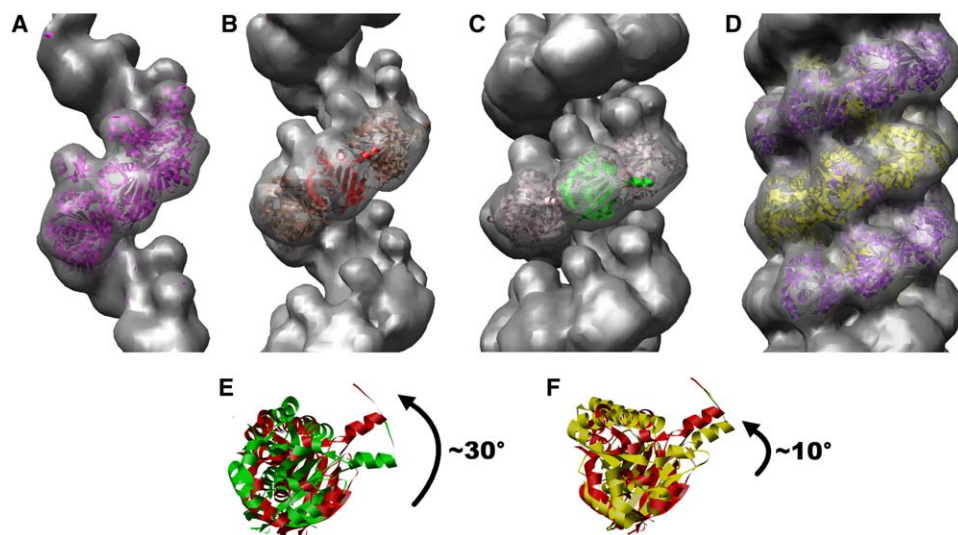


Figure 4. Three-Dimensional Reconstructions of RadA-S2G Filaments

Filaments formed in the presence of ADP-AIF (B) and AMP-PNP (C) show up as one-start helices, while RadA- Δ 62 produces a two-start helix in the presence of ATP-AIF (D). Filament in (B) has a pitch of ~ 99 Å, while filament in (C) is in the compressed form having a pitch of ~ 71 Å. A crystal structure of the “core” part (residues 63–322) of MvRadA was used to explore the orientation of protomers in these reconstructions, and this orientation was compared with the “crystal” filament shown in (A). No difference was found in the orientation of the protomers between the “crystal” filament (A) and RadA-S2G-ADP-AIF filament (B), except N terminus in (B) was not fully visualized due to partial disorder. Protomers within RadA-AMP-PNP filament were rotated by $\sim 30^\circ$ (E, green ribbon) from their position in the extended filaments (E, red ribbon). The subunits that are shown in (E) correspond to those in the centers of (B) and (C), and the rotation is thus about an axis that is perpendicular to the filament axis. The orientation of the protomers in the two-start helix produced by RadA- Δ 62 (F, yellow ribbon) was close to the orientation found in Rad-S2G-ADP-AIF complex (F, red ribbon).

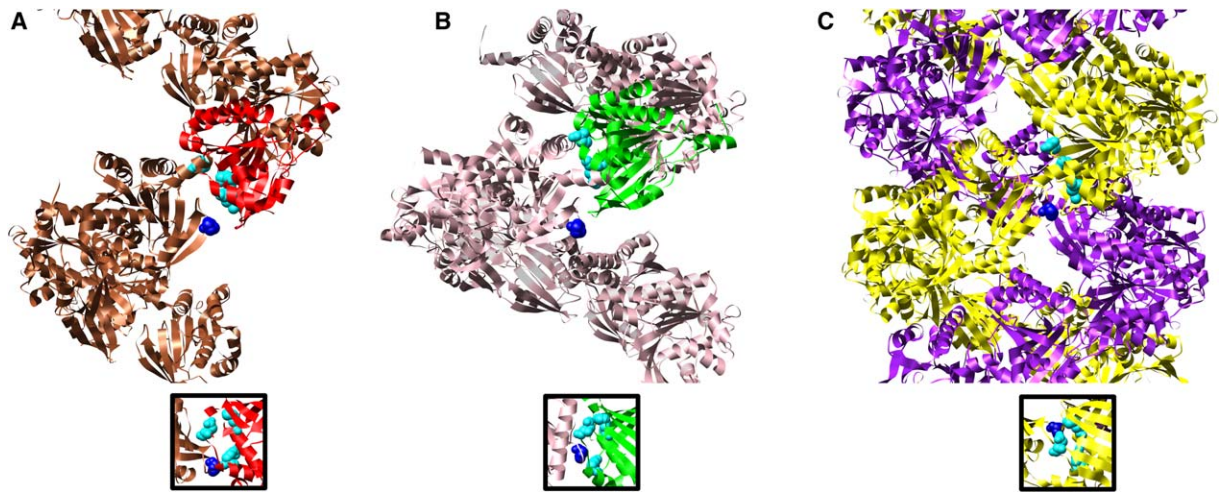


Figure 5. RadA Residues Involved in ATP Hydrolysis

The positions of these residues (Wu et al., 2004) in extended RadA-ADP-AIF filaments (A), compressed RadA-AMP-PNP filaments (B), and the two-stranded RadA- Δ 62-ATP-AIF filaments (C). Residues Arg-158 (cyan) and Pro-307 (blue), which tether the base, and Lys-111 (cyan) and Glu-151 (cyan), needed for catalysis, are shown as ball-and-stick models. The distances between the C α atoms of Pro-307 and Arg-158 are: RadA-ADP-AIF, 9.4 Å; RadA-AMP-PNP, 19.0 Å; RadA- Δ 62-ATP-AIF, 12.2 Å.

filament (Figure 7C) show that the N-terminal domain is seen in the wild-type filament but missing in the G103E mutant. We have used a second preparation of both the G103E mutant and the wild-type protein to generate new EM images and three-dimensional reconstructions to independently confirm these observations. The result with the wild-type protein was surprising because the first three-dimensional reconstruction failed to visualize an N-terminal domain (Ogawa et al., 1993; Yu et al., 2001), presumably due to large disorder, while this

N-terminal domain is clearly seen in the filaments formed by human Rad51. We suggest that the failure to visualize the N-terminal domain in the original studies of yeast Rad51 (Ogawa et al., 1993) was due to the inactivity of that protein and that, under conditions where the protein is active, yeast Rad51 generates very similar filaments to those formed by human Rad51. Also the absence of the N terminus in the reconstruction of the Rad51-G103E mutant was surprising because it had been hypothesized that E103 makes a new contact with a positively

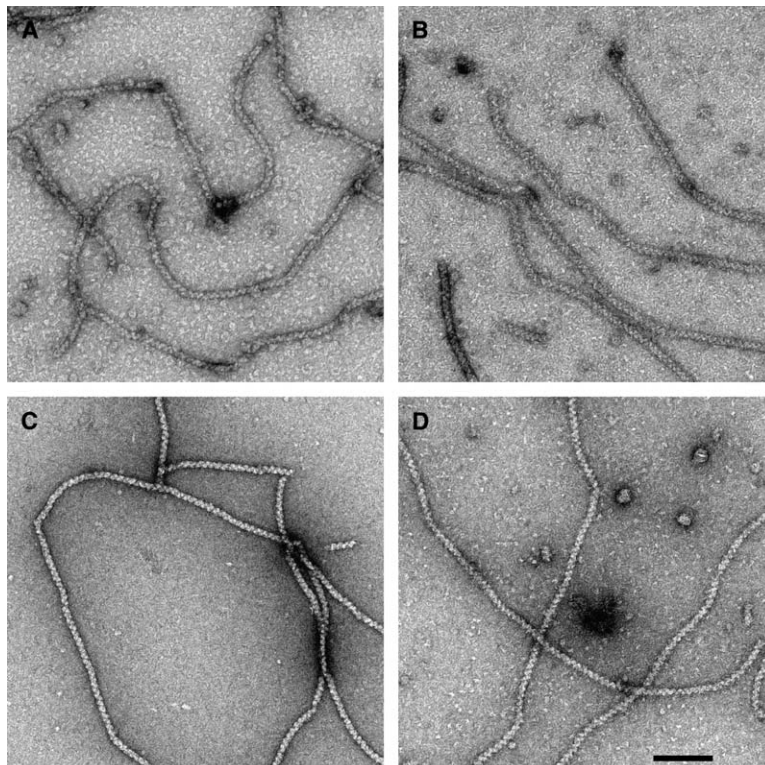


Figure 6. Electron Micrographs of Yeast Rad51

The wild-type protein forms filaments on dsDNA in the presence of the ATP analogs AMP-PNP (A) or ATP- γ -S (B), while the G103E mutant failed to polymerize under these conditions. In the presence of ATP and aluminum fluoride, both the wild-type protein (C) and the G103E mutant (D) formed long filaments on dsDNA. The scale bar is 1000 Å.

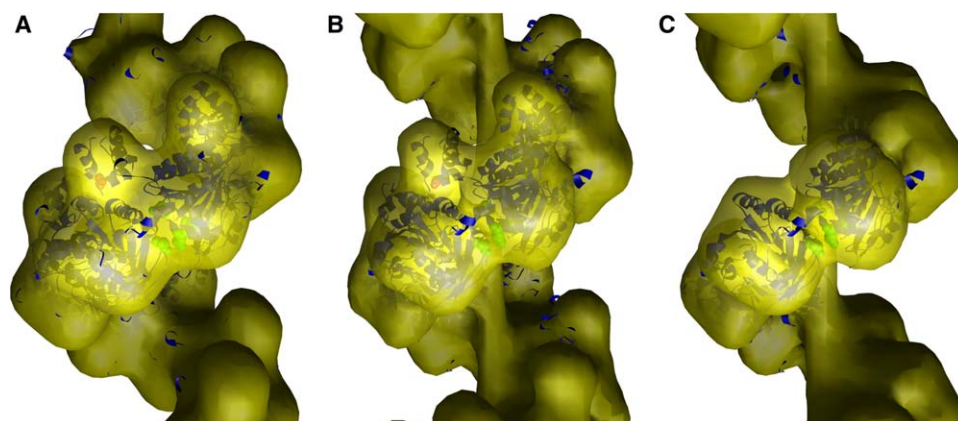


Figure 7. The Yeast Rad51 Filament

Three-dimensional reconstructions of yeast Rad51-DNA filaments (B and C) and a crystal structure (Conway et al., 2004) of the protein (A). The wild-type Rad51-DNA filament (B) is quite similar to the crystal filament (A), while the G103E mutant forms a filament on DNA in which the N-terminal domain is not visualized after averaging (C).

charged patch on the helical domain of the ATPase core formed by R260, H302, and K305 that could lock the N terminus to the core (Zhang et al., 2005). It is unclear whether the N terminus in Rad51-G103E is disordered or present in multiple states that preclude its visualization. We note that in the wild-type protein G103 and H105 contact D263 on the ATPase core domain, an interaction that can be expected to be weakened in the G103E mutant protein.

We have fit the crystal structure of yeast Rad51 (Conway et al., 2004) into our EM reconstructions. The crystal of yeast Rad51 contained a helical filament with a pitch of 130 Å, but it can be seen that the crystal filament (Figure 7A) matches quite well the reconstruction of the extended Rad51-DNA filament that has a pitch of 99 Å (Figure 7B). The filament formed by RAD51-G103E has an ATPase core that appears to be in a similar orientation to that in the active, extended wild-type Rad51 filament. The question is then why does the G103E mutant fail to hydrolyze ATP? A likely explanation is that each subunit in this filament might hydrolyze ATP, but turnover is prevented by the absence of a fixed N-terminal domain to stabilize the transition between the two conformational states of the filament (and subunits). In RadA, we have shown (above) that the N-terminal domain makes a contact with the ATPase core of an adjacent subunit in the extended state, which we suggest plays an important role in the ATPase cycle. Consistent with this prediction, an initial burst of ATPase activity is seen with the G103E mutant, followed by a decline in activity, while the wild-type protein shows steady state ATPase activity (Figure 8).

Discussion

We have used archaeal RadA and yeast Rad51 to examine the role of the N-terminal domain in filament formation, ATP hydrolysis, and DNA strand exchange. Deletion of the N-terminal domain in RadA, and the G103E mutation in RAD51's N-terminal domain, inactivate the proteins for DNA strand exchange. We can show that both proteins form filaments on DNA under the appropri-

ate conditions, but these conditions are more restrictive for G103E than for the wild-type Rad51. In the presence of the ATP analogs ATP- γ -S or AMP-PNP, the wild-type Rad51 forms filaments on DNA, while the G103E mutant fails to polymerize. Since we know that residue 103 is far from the site of nucleotide binding in the filament (Conway et al., 2004), there cannot be a direct interaction between the nucleotide and the glutamic acid that has been substituted at residue 103. An interaction occurs between the N-terminal domain of one subunit and the nucleotide binding core of an adjacent subunit, which we have directly visualized in both the wild-type yeast Rad51 filament reconstruction (Figure 6B) and for the wild-type RadA filament (Figure 4B). These interactions between the N-terminal domain of one subunit and the ATP binding core of an adjacent subunit have also been visualized in high-resolution crystal structures of the extended filaments formed by both RadA (Wu et al., 2004) and Rad51 (Conway et al., 2004). We have shown that the G103E mutation leads to disorder in the N-terminal domain, and we suggest that for yeast

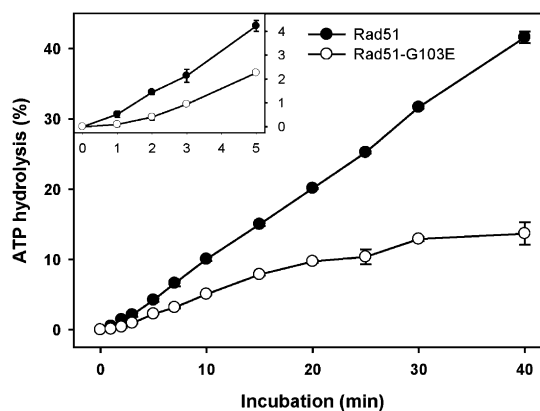


Figure 8. ATPase Activity of Wild-Type and G103E Mutant Yeast Rad51 Protein

The initial activity seen with the G103E mutant, followed by a plateau showing no further activity, is consistent with a single hydrolytic event with no subsequent turnover.

Rad51, a proper contact between the N-terminal domain and the core of an adjacent subunit is needed for filament formation in the presence of the analogs ATP- γ -S or AMP-PNP. For archaeal RadA, we have found that in the absence of the N-terminal domain (RadA- Δ 62) compressed filaments can be formed on DNA in the presence of AMP-PNP.

In the presence of ATP, the Rad51-G103E protein can form filaments on DNA, as can the RadA- Δ 62 fragment that is missing an N-terminal domain. We suggest, however, that normal hydrolysis of ATP by this filament requires a proper coordination between the N-terminal domain of one subunit and the ATP binding core of an adjacent subunit. Why, then, is the filament formed by RadA- Δ 62, completely lacking an N-terminal domain, active in ATP hydrolysis, while the RAD51-G103E filament is not? We have shown that the predominant filament formed on DNA by RadA- Δ 62 in the presence of ATP is not the normal one-start helix with \sim six subunits per turn but rather a two-start helix, with each strand having \sim eight subunits per turn. Within this two-stranded filament, each nucleotide binding core makes contact with four adjacent subunits, in contrast to each subunit making contact with two adjacent subunits in the normal one-start helix. The ability of these strands to slip with respect to each other is probably crucial for the turnover in the ATPase cycle, as subunits rotate between the “inactive” and “active” orientations. We suggest that the new contacts that appear in the two-start structure can allow for the proper coordination and hydrolysis of ATP in the absence of an N-terminal domain. Not surprisingly the two-start helical filament is inactive in DNA strand exchange.

The flexibility of the N-terminal domain in the archaeal RadA and eukaryotic Rad51/Dmc1 family of proteins is now firmly established. A crystal structure of a heptameric ring formed by one archaeal RadA (Pfrad51) contained only one N-terminal domain, as the other six N-terminal domains were disordered in the crystal (Shin et al., 2003). Fitting the Pfrad51 crystal subunit into an EM reconstruction of the *Sulfolobus solfataricus* RadA-DNA filament (Yang et al., 2001) required a rotation of the N-terminal domain by \sim 60° and a translation by \sim 20 Å (Shin et al., 2003). A crystal structure of an octameric ring formed by the human Dmc1 protein did not contain any N-terminal domains, as they were all disordered (Kinebuchi et al., 2004). Electron microscopic observations have suggested an even greater degree of flexibility and disorder (Yu et al., 2001). In the crystal structures, movements of the N-terminal domain by \sim 2–4 Å would be enough to weaken or eliminate interpretable electron density. For the N-terminal domain to vanish at \sim 20 Å resolution, as shown previously in EM reconstructions for certain states of the *Sulfolobus solfataricus* RadA-DNA filament (Yang et al., 2001) and as shown in this paper for yeast Rad51-G103E-DNA filaments, the N-terminal domain must be making movements with amplitudes on the order of 20 Å or greater.

Given these observations, it is interesting to consider that the BRC3 repeat within BRCA2 has been shown to bind to the N-terminal domain of human Rad51 protein within Rad51-DNA filaments (Galkin et al., 2005). Mutations in BRCA2 have been linked with an increased risk of cancer, and BRCA2 has been shown to recruit

Rad51 to sites of DNA damage (Powell and Kachnic, 2003). Given that the G103E mutation in yeast Rad51 destabilizes the N-terminal domain and eliminates both the in vitro ATPase and DNA strand-exchange activities, it is tempting to speculate that the binding of BRCA2 to the human Rad51 N-terminal domain is the basis for the nucleation and regulation of Rad51-DNA filaments at the site of DNA damage. While there are many caveats that are needed in extrapolating from yeast Rad51 to human Rad51, including the additional residues that are present at the N terminus of the yeast protein, this is a testable model that should serve as the basis for further experiments both in vitro and in vivo.

Experimental Procedures

RadA Protein Preparation and Crystallization

Full-length RadA from *M. voltae* was cloned into pET19 as reported (Reich et al., 2001). The ORF was amplified by PCR by using *pfu* polymerase (Fermentas) with a pair of primers (Integrate DNA Technologies): RADAS2GncolFor (CATGccatgg GTGATAATTT AACTG ATTTG CC) and RADAXholRev (CCGctcgagT TAATCTTGAA TACCT TTTTC AG). The coding sequence for amino acid sequence 63–322 of *M. voltae* RadA was amplified with primers (IDT DNA) Δ 62RADANdelFor (GAGATTTATG TcatatgGGTT TAAAAGTGG TATTG) and RADAXholRev. The coding sequences were inserted into pET28a (Novagen) by double digestion and ligation. The resultant plasmids were used to transform BL21-Codon-Plus-RIL(DE3) cells (Stratagene). Transformed cells were grown at 37°C in the presence of 35 mg/l each of kanamycin and chloramphenicol. IPTG was added to 0.25 mM when cell density reached an OD₆₀₀ between 0.5 and 0.8. The cells were harvested 4 hr after IPTG induction and then sonicated. Both proteins were found in the supernatant after centrifugation. The recombinant full-length protein carrying a S2G mutation was purified as described (Wu et al., 2004). The Δ 62RadA protein fused with an N-terminal hexa-histidyl tag was purified by Ni-affinity chromatography (Novagen manual). The fusion tag was removed by over-night thrombin digestion at 4°C, and the resultant protein with four extra N-terminal residues (Gly-Ser-His-Met) was further purified by gel filtration with an isocratic solution of 0.5 M NaCl and 30 mM of Tris-HCl buffer (pH 7.9). Both purified proteins were concentrated to \sim 30 mg/ml by ultrafiltration.

The hanging drop method was employed to crystallize the Δ 62RadA protein at a room temperature of 21°C. The optimal well solution had a composition of 2 mM AMP-PNP (Sigma-Aldrich), 0.05 M MgCl₂, 0.2 M NaCl, and 20% PEG 400 (Sigma) and 0.05 M Tris-HCl (pH 7.5). The crystals grew to a maximum size of 0.05 mm \times 0.05 mm \times 0.2 mm in a week. Harvested crystals were gradually transferred to stabilization solutions composed of the well solution supplemented by 5%, 10%, 15%, 20%, and 25% glycerol and then flash cooled to 100 K in a nitrogen stream generated by an Oxford CryoSystem device. The 0.4° oscillation images were acquired and processed with a Bruker Proteum-R system as described (Wu et al., 2004). The counterpart in the previously solved MvRadA model (PDB entry 1T4G) was employed as the search model to solve the structure by the molecular replacement method implemented in AMoRe (Navaza, 2001). Each model was iteratively rebuilt with XtalView (McRee, 1999) and refined by CNS (Brunger et al., 1998). Statistics of the diffraction data, refinement, and geometry are shown in Table 2. The molecular figures were generated with Molscript (Kraulis, 1991) and PyMOL (DeLano Scientific). The coordinates and structure factors have been deposited in the Protein Data Bank (PDB entry 2GDJ).

RadA DNA Strand-Exchange Assay

The DNA substrates were chosen from a published study (Mazin et al., 2000). Three oligonucleotides (#1, 63-nt, ACAGCACCAG ATTC AGCAAT TAAGTCTAA GCCATCCGCA AAAATGACCT CTTATCAAA A GGA; #45, 31-nt, ACAGCACCAG ATTCAGCAAT TAAGTCTAA G; #55, 31-nt, CTTAGAGCTT AATTGCTGAA TCTGGTGCTG T) were obtained from Integrated DNA Technologies. Equal molarities of complementary oligonucleotides #45 and #55 were heated at 95°C for

Table 2. X-Ray Crystallographic Data and Structure Refinement Statistics

X-Ray Crystallographic Data (Cu K α)	
Radiation, Wavelength = 1.5418 Å; Space Group P6 ₁	
Unit cell dimensions (Å)	a, b = 67.8; c = 91.1
Resolution range ^a (Å)	2.5 (2.6–2.5)
Observed reflections	31,660
Unique reflection	7,410
Completeness	89.7% (63.6%)
R _{sym} ^b	0.052 (0.309)
I/ σ	11.8/2.1
Crystal Structure Refinement	
Reflection with F > 0	7,000/84.9%
R factor/free R ^c	0.210/0.268
Contents	237 amino acids, 1 AMP-PNP, 2 Mg ²⁺
Rmsd: bond/angle	0.0075 Å/1.29°
Ramachandran	
Most favored	89.0%
Disallowed	0

^a Values in parentheses refer to values in the highest resolution shell.

^b $R_{\text{sym}} = \sum |I_h - \langle I \rangle_h| / \sum I_h$, where $\langle I \rangle_h$ is average over symmetry equivalents, and h is reflection index.

^c R factor = $\sum |F_{\text{obs}} - F_{\text{calc}}| / \sum F_{\text{obs}}$. The free R factor is calculated with a randomly selected 5% of the reflections set aside throughout the refinement.

5 min and then slowly cooled down to generate the dsDNA substrate. The solution for DNA strand-exchange reaction was composed of 3 mM ATP or an analogous nucleoside triphosphate, 10 mM MgCl₂, 100 mM KCl, 50 mM HEPES-Tris buffer (pH 7.4), 20 μ M RadA, and 1 μ M oligonucleotides. The 63 nt ssDNA substrate (oligonucleotide #1) was preincubated at 37°C with RadA for 1 min before adding the dsDNA substrate. The reaction was stopped at 30 min by adding EDTA to a concentration of 20 mM and trypsin to a concentration of 1 μ g/ μ l. After 10 min of trypsin digestion, a 10 μ l sample was mixed with 5 μ l of a loading buffer composed of 30% glycerol and 0.1% bromophenol blue and then loaded onto a 17.5% acrylamide gel. The SDS-PAGE was developed, stained with ethidium bromide, and visualized with an UV illuminator. An optional ATP regeneration system was used as specified, which was composed of 6 mM of phosphoenolpyruvate and 0.01 unit/ μ l of pyruvate kinase (New England Biolabs).

RadA ATPase Assay

A solution containing 0.033% w/v Malachite Green, 1.3% w/v ammonium molybdate, and 1.0 M HCl was used to monitor the release of inorganic phosphate from ATP hydrolysis (Itaya and Ui, 1966). Absorbance at 620 nm was recorded for quantification. The reaction solutions for the DNA-dependent ATPase assay contained 3 μ M RadA, 18 μ M ssDNA (in nucleotides) or dsDNA (in base pairs), 5 mM ATP, 0.05 M Tris-HEPES buffer (pH 7.4), 10 mM MgCl₂, 100 mM of KCl, and 0.1% v/v 2-mercaptoethanol. Solutions without RadA were taken as absorbance references. A 36-nt oligonucleotides poly-(dT)₃₆ (Integrated DNA Technologies) was used as the ssDNA substrate in this assay. Full-length ϕ X174 DNA (New England Biolabs) linearized by Pst I digestion was used as the dsDNA substrate.

Rad51 ATPase Assay

The wild-type and G103E mutant Rad51 proteins were prepared as described (Zhang et al., 2005). ATPase activity was analyzed by TLC, incubated at 30°C as described (Seitz et al., 1998). The reaction buffer contained 33 mM Tris-HCl (pH 7.5), 13 mM MgCl₂, 1.8 mM DTT, 1 mM ATP, and 90 μ g/ml BSA (Zhang et al., 2005). In a 50 μ l reaction, Rad51 and poly(dT) ssDNA were 2 μ M and 24 μ M, respectively (stoichiometry 1:12). The reaction was started by adding 2.5 μ l [γ -³²P]ATP solution (containing 10 mM Tris-HCl [pH 7.5],

9.6 mM ATP, and 0.385 μ Ci/ μ l [γ -³²P]ATP). At the time points indicated, 2.5 μ l reaction volume was withdrawn and mixed with 1.25 μ l stop solution (contains 6.7 mM ATP, 6.7 mM ADP, and 33.3 mM EDTA). One microliter of the final mixture was spotted on cellulose PEI-F TLC plate (J.T.Baker). The free radioactive phosphate was separated from nonhydrolyzed radioactive ATP by running the TLC plate in a solution containing 0.8 M LiCl and 1 M formic acid. The plate was dried and exposed to a phosphorimager plate and quantified with Storm 840 and Imagequant 5.2 software (GE Healthcare).

Complex Formation and Electron Microscopy

All complexes were formed in 25 mM Triethanolamine-HCl (Fisher) buffer (pH 7.2).

Preparation of mvRadA-S2G or mvRadA- Δ 62 with dsDNA and ADP and Aluminum Fluoride Complexes

Incubation at 37°C for 30 min, with mvRadA Δ 62 (or mvRadA Δ 62) concentration of 3 μ M, protein to calf thymus dsDNA (Sigma) ratio of 40:1 (w/w), ADP (Sigma) 1.25 mM, magnesium acetate (Sigma) 2 mM, NaF (Aldrich) 1.25 mM, and Al(NO₃)₃ (Aldrich) 1.25 mM.

Preparation of mvRadA-S2G or mvRadA- Δ 62 with dsDNA and AMP-PNP Complexes

Incubation was at 37°C for 10 min, with mvRadA concentration of 3 μ M, protein to thymus dsDNA (Sigma) ratio of 40:1 (w/w), AMPNP (Sigma) 2.5 mM, and magnesium acetate (Sigma) 2 mM.

Preparation of mvRadA- Δ 62 with ssDNA and ATP and Aluminum Fluoride Complexes

Incubation was at 37°C for 30 min, with mvRadA- Δ 62 concentration of 3 μ M, protein to M13 ssDNA (Sigma) ratio of 80:1 (w/w), ATP (Sigma) 1.25 mM, magnesium acetate (Sigma) 10 mM, KCl (J.T.Baker) 100 mM, NaF (Aldrich) 1.25 mM, and Al(NO₃)₃ (Aldrich) 1.25 mM.

Preparation of Rad51 or Rad51-G103E with dsDNA and ATP and Aluminum Fluoride

Incubation was at 25°C for 15 min, with Rad51 concentration of 1.5 μ M, protein to thymus dsDNA (Sigma) ratio of 40:1 (w/w), ATP (Sigma) 1.25 mM, magnesium acetate (Sigma) 10 mM. After this initial incubation, NaF (Aldrich) and Al(NO₃)₃ (Aldrich) were added to a final concentration of 1.25 mM and incubated at 25°C for an additional 30 min.

Preparation of Rad51 or Rad51-G103E with dsDNA and AMP-PNP or ATP γ S Complexes

Incubation was at 25°C for 15 min, with Rad51 (or Rad51-G103E) concentration of 1.5 μ M, protein to thymus dsDNA (Sigma) ratio of 40:1 (w/w), AMP-PNP (Sigma) or ATP γ S (Boehringer) 1.25 mM, magnesium acetate (Sigma) 10 mM.

Samples were applied to carbon-coated grids and stained with 2% uranyl acetate (w/v). Images were recorded on film with a Tecnai 12 electron microscope operating at 80 keV with a nominal magnification of 30,000 \times . Negatives were scanned with a Nikon Coolscan 8000 densitometer at a raster of 4.2 Å/pixel.

Image Analysis

MvRadA-ADP-AIF-dsDNA Filaments

We extracted 945 segments, each 60 \times 110 pixels. From each segment, five overlapping boxes, each 60 \times 60 pixels, were extracted to form a set of 4725 images. The IHSRS method (Egelman, 2000) was used to make an overall reconstruction of the set. To evaluate the quality of the raw images, each set of five overlapping segments was cross-correlated with projections of the reconstruction. Only sets having at least four segments with the same polarity were retained to create a new set of 2880 images. To sort these segments by pitch, we created a set of 11 model volumes having pitch values from 75–125 Å with a step size of 5 Å, and these were cross correlated with the images. By this method, 2051 filament segments having a pitch from 90–100 Å were used for the final reconstruction. After 60 iterations, the structure converged to a symmetry of 57.6° rotation per subunit and an axial rise of 15.8 Å per subunit.

MvRadA-AMP-PNP-dsDNA Filaments

Similar reconstruction procedures were used for these as described above. The 3340 image segments with the best polarity were cross correlated with projections of model volumes having a pitch of either 64, 71, or 79 Å. Segments assigned to the 71 Å pitch class (n = 1864) were reconstructed and yielded a symmetry of 50.0° per subunit with an axial rise of 9.9 Å per subunit.

MvRadA-Δ62-ATP-AIF-ssDNA

The appearance of the filaments formed by this fragment in the presence of ATP-AIF was quite different from that of the full length MvRadA, and analysis of diffraction patterns showed that the layer line at $\sim 1/50$ Å contained a Bessel order $n = 2$. By using the IHRSR procedure, a stable solution was found for a symmetry of 157° per subunit, with an axial rise of 6.2 Å, which corresponds to a two-stranded helical structure with \sim eight subunits per turn of each 100 Å pitch strand. The two strands are shifted axially with respect to each other by exactly half the rise per subunit along one strand. Indications existed that the relationship between the strands was variable within the data set. To improve the reconstruction, we created model volumes having different shifts and rotations between the two strands, and these were cross correlated with 3855 images. Only the 1235 segments that yielded the best correlation with the symmetrical two-stranded structure described (a 180° rotation between the strands, with an axial shift of one-half of the subunit rise) were used for the final reconstruction. This yielded a symmetry of 157.2° and an axial rise of 6.3 Å.

Wild-Type Rad51

We collected 5635 segments (each 60×60 pixels) and sorted these by pitch by using the procedure described for MvRadA-ADP-AIF-ssDNA (see above). Segments having a pitch of 90–100 Å ($n = 3379$) were used for the final reconstruction, which yielded a symmetry of 56.2° with an axial rise of 15.5 Å.

Rad51-G103E

The same approach was used for the Rad51-G103E protein, with 5250 segments collected and 3379 images having a pitch of 90–100 Å included in the final reconstruction. The symmetry converged to 56.1° with an axial rise of 15.5 Å.

Acknowledgments

We thank the Saskatchewan Structural Sciences Centre for access to its X-ray facility. This work was supported by Natural Sciences and Engineering Research Council of Canada, Saskatchewan Health Research Foundation, and Canadian Institutes of Health Research (Y.L.) and National Institutes of Health GM58015 (W.D.H.) and GM35269 (E.H.E.). X.P.Z. is a Susan G. Komen Breast Cancer Foundation postdoctoral fellow (PDF403213). Y.L. is a CIHR New Investigator.

Received: February 24, 2006

Revised: April 8, 2006

Accepted: April 10, 2006

Published: June 13, 2006

References

Aboussekhra, A., Chanet, R., Adjiri, A., and Fabre, F. (1992). Semi-dominant suppressors of Srs2 helicase mutations of *Saccharomyces cerevisiae* map in the RAD51 gene, whose sequence predicts a protein with similarities to procaryotic RecA proteins. *Mol. Cell Biol.* **12**, 3224–3234.

Abrahams, J.P., Leslie, A.G., Lutter, R., and Walker, J.E. (1994). Structure at 2.8 Å resolution of F_1 -ATPase from bovine heart mitochondria. *Nature* **370**, 621–628.

Aihara, H., Ito, Y., Kurumizaka, H., Terada, T., Yokoyama, S., and Shibata, T. (1997). An interaction between a specified surface of the C-terminal domain of RecA protein and double-stranded DNA for homologous pairing. *J. Mol. Biol.* **274**, 213–221.

Aihara, H., Ito, Y., Kurumizaka, H., Yokoyama, S., and Shibata, T. (1999). The N-terminal domain of the human Rad51 protein binds DNA: structure and a DNA binding surface as revealed by NMR. *J. Mol. Biol.* **290**, 495–504.

Brunger, A.T., Adams, P.D., Clore, G.M., DeLano, W.L., Gros, P., Grosse-Kunstleve, R.W., Jiang, J.S., Kuszewski, J., Nilges, M., Pannu, N.S., et al. (1998). Crystallography & NMR system: a new software suite for macromolecular structure determination. *Acta Crystallogr. D Biol. Crystallogr.* **54**, 905–921.

Clark, A.J., and Margulies, A.D. (1965). Isolation and characterization of recombination-deficient mutants of *Escherichia coli* K12. *Proc. Natl. Acad. Sci. USA* **53**, 451–459.

Conway, A.B., Lynch, T.W., Zhang, Y., Fortin, G.S., Fung, C.W., Symington, L.S., and Rice, P.A. (2004). Crystal structure of a Rad51 filament. *Nat. Struct. Mol. Biol.* **11**, 791–796.

Courcelle, J., Khodursky, A., Peter, B., Brown, P.O., and Hanawalt, P.C. (2001). Comparative gene expression profiles following UV exposure in wild-type and SOS-deficient *Escherichia coli*. *Genetics* **158**, 41–64.

Datta, S., Prabu, M.M., Vaze, M.B., Ganesh, N., Chandra, N.R., Muniyappa, K., and Vijayan, M. (2000). Crystal structures of *Mycobacterium tuberculosis* RecA and its complex with ADP-AIF(4): implications for decreased ATPase activity and molecular aggregation. *Nucleic Acids Res.* **28**, 4964–4973.

Datta, S., Ganesh, N., Chandra, N.R., Muniyappa, K., and Vijayan, M. (2003a). Structural studies on MtRecA-nucleotide complexes: insights into DNA and nucleotide binding and the structural signature of NTP recognition. *Proteins* **50**, 474–485.

Datta, S., Krishna, R., Ganesh, N., Chandra, N.R., Muniyappa, K., and Vijayan, M. (2003b). Crystal structures of *Mycobacterium smegmatis* RecA and its nucleotide complexes. *J. Bacteriol.* **185**, 4280–4284.

Egelman, E.H. (2000). A robust algorithm for the reconstruction of helical filaments using single-particle methods. *Ultramicroscopy* **85**, 225–234.

Galkin, V.E., Esashi, F., Yu, X., Yang, S., West, S.C., and Egelman, E.H. (2005). BRCA2 BRC motifs bind RAD51-DNA filaments. *Proc. Natl. Acad. Sci. USA* **102**, 8537–8542.

Itaya, K., and Ui, M. (1966). A new micromethod for the colorimetric determination of inorganic phosphate. *Clin. Chim. Acta* **14**, 361–366.

Kinebuchi, T., Kagawa, W., Enomoto, R., Tanaka, K., Miyagawa, K., Shibata, T., Kurumizaka, H., and Yokoyama, S. (2004). Structural basis for octameric ring formation and DNA interaction of the human homologous-pairing protein Dmc1. *Mol. Cell* **14**, 363–374.

Kowalczykowski, S.C., and Eggleston, A.K. (1994). Homologous pairing and DNA strand-exchange proteins. *Annu. Rev. Biochem.* **63**, 991–1043.

Kraulis, P.J. (1991). MOLSCRIPT: a program to produce both detailed and schematic plots of protein structures. *J. Appl. Crystallogr.* **24**, 946–950.

Mazin, A.V., Zaitseva, E., Sung, P., and Kowalczykowski, S.C. (2000). Tailed duplex DNA is the preferred substrate for Rad51 protein-mediated homologous pairing. *EMBO J.* **19**, 1148–1156.

McRee, D.E. (1999). XtalView/Xfit—a versatile program for manipulating atomic coordinates and electron density. *J. Struct. Biol.* **125**, 156–165.

Navaza, J. (2001). Implementation of molecular replacement in AMoRe. *Acta Crystallogr. D Biol. Crystallogr.* **57**, 1367–1372.

Ogawa, T., Yu, X., Shinohara, A., and Egelman, E.H. (1993). Similarity of the yeast RAD51 filament to the bacterial RecA filament. *Science* **259**, 1896–1899.

Pellegrini, L., Yu, D.S., Lo, T., Anand, S., Lee, M., Blundell, T.L., and Venkitaraman, A.R. (2002). Insights into DNA recombination from the structure of a RAD51-BRCA2 complex. *Nature* **420**, 287–293.

Powell, S.N., and Kachnic, L.A. (2003). Roles of BRCA1 and BRCA2 in homologous recombination, DNA replication fidelity and the cellular response to ionizing radiation. *Oncogene* **22**, 5784–5791.

Rajan, R., and Bell, C.E. (2004). Crystal structure of RecA from *Deinococcus radiodurans*: insights into the structural basis of extreme radioresistance. *J. Mol. Biol.* **344**, 951–963.

Reich, C.I., McNeil, L.K., Brace, J.L., Brucker, J.K., and Olsen, G.J. (2001). Archaeal RecA homologues: different response to DNA-damaging agents in mesophilic and thermophilic Archaea. *Extremophiles* **5**, 265–275.

Sandler, S.J., Satin, L.H., Samra, H.S., and Clark, A.J. (1996). recA-like genes from three archaean species with putative protein products similar to Rad51 and Dmc1 proteins of the yeast *Saccharomyces cerevisiae*. *Nucleic Acids Res.* **24**, 2125–2132.

Schlacher, K., Leslie, K., Wyman, C., Woodgate, R., Cox, M.M., and Goodman, M.F. (2005). DNA polymerase V and RecA protein, a minimal mutasome. *Mol. Cell* **17**, 561–572.

- Sehorn, M.G., Sigurdsson, S., Bussen, W., Unger, V.M., and Sung, P. (2004). Human meiotic recombinase Dmc1 promotes ATP-dependent homologous DNA strand exchange. *Nature* **429**, 433–437.
- Seitz, E.M., Brockman, J.P., Sandler, S.J., Clark, A.J., and Kowalczykowski, S.C. (1998). RadA protein is an archaeal RecA protein homolog that catalyzes DNA strand exchange. *Genes Dev.* **12**, 1248–1253.
- Shin, D.S., Pellegrini, L., Daniels, D.S., Yelent, B., Craig, L., Bates, D., Yu, D.S., Shivji, M.K., Hitomi, C., Arvai, A.S., et al. (2003). Full-length archaeal Rad51 structure and mutants: mechanisms for RAD51 assembly and control by BRCA2. *EMBO J.* **22**, 4566–4576.
- Shinohara, A., Ogawa, H., and Ogawa, T. (1992). Rad51 protein involved in repair and recombination in *S. cerevisiae* is a RecA-like protein. *Cell* **69**, 457–470.
- Story, R.M., Weber, I.T., and Steitz, T.A. (1992). The structure of the *E. coli* recA protein monomer and polymer. *Nature* **355**, 318–325.
- VanLoock, M.S., Yu, X., Yang, S., Lai, A.L., Low, C., Campbell, M.J., and Egelman, E.H. (2003). ATP-mediated conformational changes in the RecA filament. *Structure* **11**, 187–196.
- Wu, Y., He, Y., Moya, I.A., Qian, X., and Luo, Y. (2004). Crystal structure of archaeal recombinase RADA: a snapshot of its extended conformation. *Mol. Cell* **15**, 423–435.
- Xing, X., and Bell, C.E. (2004a). Crystal structures of *Escherichia coli* RecA in complex with MgADP and MnAMP-PNP. *Biochemistry* **43**, 16142–16152.
- Xing, X., and Bell, C.E. (2004b). Crystal structures of *Escherichia coli* RecA in a compressed helical filament. *J. Mol. Biol.* **342**, 1471–1485.
- Yang, S., Yu, X., Seitz, E.M., Kowalczykowski, S.C., and Egelman, E.H. (2001). Archaeal RadA protein binds DNA as both helical filaments and octameric rings. *J. Mol. Biol.* **314**, 1077–1085.
- Yu, X., Jacobs, S.A., West, S.C., Ogawa, T., and Egelman, E.H. (2001). Domain structure and dynamics in the helical filaments formed by RecA and Rad51 on DNA. *Proc. Natl. Acad. Sci. USA* **98**, 8419–8424.
- Zhang, X.P., Lee, K.I., Solinger, J.A., Kiianitsa, K., and Heyer, W.D. (2005). Gly-103 in the N-terminal domain of *Saccharomyces cerevisiae* Rad51 protein is critical for DNA binding. *J. Biol. Chem.* **280**, 26303–26311.

Accession Numbers

The coordinates and structure factors for RadA- Δ 62 have been entered into the Protein Data Bank with the accession number 2GDJ.